PFC/JA-89-26

LINEAR THEORY OF THE COLLECTIVE RAMAN INTERACTION IN A FREE-ELECTRON LASER WITH A PLANAR WIGGLER AND AN AXIAL GUIDE FIELD

by

H.P. Freund,* R.C. Davidson and G.L. Johnston

May, 1989

Plasma Fusion Center
Massachusetts Institute of Technology
Cambridge, MA 02139

*Permanent Address: Science Applications International Corporation, McLean, VA 22102.

Research supported in part by the Office of Naval Research, in part by the National Science Foundation, and in part by the Naval Research Laboratory Plasma Physics Division.

LINEAR THEORY OF THE COLLECTIVE RAMAN INTERACTION IN A FREE-ELECTRON LASER WITH A PLANAR WIGGLER AND AN AXIAL GUIDE FIELD

H.P. Freund,[†] R.C. Davidson, and G.L. Johnston
Plasma Fusion Center
Massachusetts Institute of Technology
Cambridge, MA 02139

ABSTRACT

A linear stability analysis of the collective Raman interaction in a Free-Electron Laser with combined planar wiggler and axial guide magnetic fields is presented. The analysis involves a perturbation of the cold-fluid model of the interaction about the single particle trajectories in the combined external fields, and the complete dispersion equation for a monoenergetic beam is obtained. In contrast to the case of a helical wiggler field in which the interaction excites a right-hand circularly polarized wave, the interaction for a planar wiggler and an axial guide field is with an elliptically polarized wave which contains both left-hand and right-hand circular components. However, the results indicate that many facets of the interaction are analogous to those found with a helical wiggler. In particular, both the transverse velocity and the growth rate of the instability tend to increase near the resonance at which the Larmor and wiggle periods coincide. In addition, a negative-mass regime is found in which the axial electron velocity increases with decreasing beam energy which drives the beam space-charge modes unstable.

[†]Permanent Address: Science Applications International Corporation, McLean, VA 22102.

I. INTRODUCTION

The physical process which gives rise to wave amplification in the Free-Electron Lasers (FEL) has been studied in depth for configurations consisting of a helical wiggler and an axial guide magnetic field. The analyses have dealt with one-dimensional[1-6] and three-dimensional[7-10] regimes in both linear stability and nonlinear simulation, and the results have been found to be in good agreement with several experiments.[11-13] The use of an axial guide field was originally conceived as a means for the enhanced focussing of intense electron beams. However, it was soon realized, as well as demonstrated experimentally, that the effect of the guide field would also be to enhance the transverse wiggler velocity and increase both the gain and efficiency of the interaction. In contrast, the preferred methods of achieving the enhanced focussing of intense beams in planar wiggler FELs have been either quadrupole magnetic fields or the parabolic tapering of the pole faces of the wiggler, and the effect of an axial guide field on the interaction in the presence of a planar wiggler have not been extensively studied.

In this paper, we present an analysis of the linear stability of a collective Raman FEL for a configuration which consists of a planar wiggler and an axial guide magnetic field. The analysis is performed for an idealized one-dimensional representation of the wiggler field, and it is implicitly assumed that the maximum displacement of the electron beam from the plane of symmetry is less than the wiggler period. One feature of the interaction that is omitted from the idealized model, however, is the existence of a $\mathbf{B}_0 \times \nabla \mathbf{B}_w$ drift. This drift is proportional to the displacement of the beam electrons from the plane of symmetry, and results in the ultimate loss of the beam to the walls of the drift tube. As a result, it is implicitly assumed in the present analysis that the beam is well confined close to the plane of symmetry. Indeed, it is important to ensure that in experiments which make use of this configuration[14] the interaction length is not long enough to account for significant expansion of the beam.

The organization of the paper is as follows. The fundamental configuration of the wiggler and guide fields are given in Sec. II along with a discussion of the single-particle orbits in the idealized wiggler representation. The perturbed orbits which result from the presence of a fluctuating electromagnetic field are discussed in Sec. III, and the source currents and charge densities are found based upon a fluid model of the interaction. The linear stability analysis in the limiting case of a vanishing axial guide field is presented in Sec. IV, and the general stability analysis appears in Sec. V. Finally, a summary and discussion is given in Sec. VI.

II. THE SINGLE-PARTICLE ORBITS

The particular configuration of interest is the propagation of an energetic electron beam through an external magnetostatic field which consists of a solenoidal guide field and a linearly polarized wiggler field which may be written in the form

$$\mathbf{B}_{ext} = B_0 \hat{\mathbf{e}}_z + B_w \hat{\mathbf{e}}_y \sin k_w z \,, \tag{1}$$

where $B_{0,w}$ denotes the magnitudes of the guide and wiggler fields respectively, and k_w is the wiggler wavenumber. This idealized one-dimensional representation for the wiggler field is valid as long as the maximum excursion of the electron from the plane of symmetry is less than λ_w (which denotes the wiggler period).

In the absence of the solenoidal field, the single-particle orbits are confined to the plane normal to the wiggler field. The effect of the solenoidal field is to impart an elliptical motion to the trajectories in the xy-plane, as well as to enhance the magnitude of the transverse velocity. These orbits can be expressed in the form

$$v_0 = v_{||}\left(\alpha_x \hat{e}_x \cos k_w z + \alpha_y \hat{e}_y \sin k_w z\right) + v_{||}\hat{e}_z \ , \tag{2}$$

where $v_{||}$ denotes the average axial velocity,

$$\alpha_x \equiv \frac{\Omega_w k_w v_{||}}{\Omega_0^2 - k_w^2 v_{||}^2} \ ,$$

$$\alpha_y \equiv \frac{\Omega_w \Omega_0}{\Omega_0^2 - k_w^2 v_{||}^2} \ , \tag{3}$$

$\Omega_{0,w} \equiv |eB_{0,w}/\gamma_0 m_e c|$, e and m_e are the electron charge and mass, and γ_0 denotes the relativistic factor corresponding to the average energy of the beam. It is evident, therefore, that the transverse components of the velocity may be significantly enhanced near the resonance at $\Omega_0 \approx k_w v_{||}$. The axial velocity can be obtained by noting that the total energy is conserved. Hence, using the average transverse velocity we obtain

$$v_{||}^2\left[1 + \frac{1}{2}\left(\alpha_x^2 + \alpha_y^2\right)\right] = \left(1 - \gamma_0^{-2}\right)c^2 \ , \tag{4}$$

which defines a cubic equation for $v_{||}^2$. It should be remarked that in using the average transverse velocity in Eq. (4), as in the idealized one-dimensional representation for the wiggler field, we are implicitly assuming that the electron beam remains close to the symmetry axis. This assures that contributions to the wiggler field and to the electron orbits which are of higher order in the wiggler field may be neglected. For example, an oscillatory contribution to the axial velocity at the second harmonic of the wiggler wavenumber is smaller than the average axial velocity $v_{||}$ by a factor of α_x^2, and may be neglected when the wiggler field is small and the resonance at $\Omega_0 \approx k_w v_{||}$ is not approached too closely. This is related to the condition that $\alpha_x^2 + \alpha_y^2 << 1$ which is required for the beam to remain close to the symmetry axis.

The solutions to Eq. (4) are symmetric with respect to the direction of propagation. This is in contrast to the orbits in the presence of a helical wiggler field[15,16] in which the direction of propagation with respect to the guide field is important and enhancements in the transverse velocity occur only for propagation parallel to the guide field. The positive branch of the solutions to Eq. (4) for $v_{||}$ are shown in Fig. 1 as functions of the solenoidal field for representative values of the wiggler field and beam energy. The results are qualitatively similar to those obtained for a helical wiggler in that two distinct groups of orbits are found corresponding to $\Omega_0 < k_w v_{||}$ (Group I) and $\Omega_0 > k_w v_{||}$ (Group II). Both orbit groups exhibit a sharp increase in the transverse velocity (and a corresponding decrease in the axial velocity) as the resonance is approached, and the Group I orbits reduce to the well-known result for an idealized planar wiggler in the absence of the guide field. In addition, it can be shown that

$$\frac{d}{d\gamma_0} v_{||} = \frac{c^2}{\gamma_0 \gamma_{||}^2 v_{||}} \Phi \ , \tag{5}$$

where $\gamma_{\|}^2 \equiv (1 - v_{\|}^2/c^2)^{-1}$, and

$$\Phi \equiv 1 - \frac{\gamma_{\|}^2 \alpha_y^2 \left(\Omega_0^2 + 3k_w^2 v_{\|}^2\right)}{2\left(\Omega_0^2 - k_w^2 v_{\|}^2\right) + \alpha_y^2 \left(\Omega_0^2 + 3k_w^2 v_{\|}^2\right)} \,. \tag{6}$$

The function Φ is plotted in Fig. 2 versus the axial guide field for parameters corresponding to both orbit groups shown in Fig. 1. It is evident that Φ approaches unity for Group I orbits in the limit in which the solenoidal field vanishes, and exhibits a singularity at the upper limit for the guide field for this orbit group. The Group II orbits exhibit more interesting behavior in that Φ is negative in the vicinity of the resonance, which implies that the orbits will undergo a negative-mass effect in that the axial velocity will increase as the beam loses energy. In fact, this negative-mass regime has been shown to give rise to an instability in the beam space-charge modes for both helical and planar wigglers.[17]

III. SOURCE CURRENTS AND CHARGE DENSITY

The source currents and charge density derived in this section are based upon a fluid analysis of the wave-particle interaction. The fundamental equations describing the beam are those of continuity

$$\frac{\partial}{\partial t} n + \nabla \cdot (n\mathbf{v}) = 0 \,, \tag{7}$$

momentum transfer

$$\frac{d}{dt} \mathbf{v} = -\frac{e}{\gamma m_e}\left[\left(\mathbf{I} - \frac{1}{c^2}\mathbf{v}\mathbf{v}\right) \cdot \delta\mathbf{E} + \frac{1}{c}\mathbf{v} \times (\mathbf{B}_{ext} + \delta\mathbf{B})\right] \,, \tag{8}$$

and energy balance

$$\frac{d}{dt} \gamma = -\frac{e}{m_e c^2} \mathbf{v} \cdot \delta\mathbf{E} \,, \tag{9}$$

where n and $\mathbf{v}$ are the macroscopic density and velocity of the beam, γ is the relativistic factor corresponding to the bulk energy of the beam, $\mathbf{I}$ is the unit dyadic, and $\delta\mathbf{E}$ and $\delta\mathbf{B}$ are the fluctuating electric and magnetic fields.

These equations are solved by means of a perturbation expansion to first order in the electromagnetic fields. We write $n = n_0 + \delta n$, $\mathbf{v} = \mathbf{v}_0 + \delta\mathbf{v}$, and $\gamma = \gamma_0 + \delta\gamma$, where the zeroth order density is constant and $(\mathbf{v}_0, \gamma_0)$ are given in terms of the single-particle orbits. All fluctuating quantities are expressed by means of Floquet's Theorem in the form

$$f(z,t) = \sum_{m=-\infty}^{\infty} f_m e^{ik_m z - i\omega t} \,, \tag{10}$$

where $k_m = k + mk_w$. The electromagnetic field is expressed in terms of the vector and scalar potentials ($\delta\mathbf{A},\delta\varphi$) in the Coulomb gauge (i.e., $\delta A_z = 0$). The perturbed quantities, therefore, satisfy the reduced equations

$$\delta n_m = n_0 \frac{k_m}{\Delta\omega_m}\,\delta v_{z,m} \ , \tag{11}$$

which describes the perturbed charge density in terms of the axial component of the perturbed velocity, and

$$\Delta\omega_m \delta v_{x,m} + i\Omega_0 \delta v_{y,m} - \frac{1}{2}\alpha_y \Omega_0 \left(\delta v_{z,m-1} - \delta v_{z,m+1}\right) = \frac{\alpha_x}{2\gamma_0} k_w v_\parallel^2 \left(\delta\gamma_{m-1} - \delta\gamma_{m+1}\right)$$

$$+ \frac{e}{\gamma_0 m_e c}\left[\left(\Delta\omega_m - \frac{\omega}{2}\alpha_x^2\beta_\parallel^2\right)\delta A_{x,m} + \frac{1}{2}\alpha_x\beta_\parallel\left(k_{m-1}v_\parallel\delta\varphi_{m-1} + k_{m+1}v_\parallel\delta\varphi_{m+1}\right)\right.$$

$$\left. - \frac{\omega}{4}\alpha_x^2\beta_\parallel^2\left(\delta A_{x,m-2} + \delta A_{x,m+2}\right) + i\,\frac{\omega}{4}\alpha_x\alpha_y\beta_\parallel^2\left(\delta A_{y,m-2} - \delta A_{y,m+2}\right)\right] \ , \tag{12}$$

$$\Delta\omega_m \delta v_{y,m} - i\Omega_0 \delta v_{x,m} + \frac{1}{2}\alpha_x \Omega_0 \left(\delta v_{z,m-1} + \delta v_{z,m+1}\right) = -\,i\,\frac{\alpha_x}{2\gamma_0}\Omega_0 v_\parallel \left(\delta\gamma_{m-1} + \delta\gamma_{m+1}\right)$$

$$+ \frac{e}{\gamma_0 m_e c}\left[\left(\Delta\omega_m - \frac{\omega}{2}\alpha_y^2\beta_\parallel^2\right)\delta A_{y,m} - \frac{i}{2}\alpha_x\beta_\parallel\left(k_{m-1}v_\parallel\delta\varphi_{m-1} - k_{m+1}v_\parallel\delta\varphi_{m+1}\right)\right.$$

$$\left. + \frac{\omega}{4}\alpha_y^2\beta_\parallel^2\left(\delta A_{y,m-2} + \delta A_{y,m+2}\right) + i\,\frac{\omega}{4}\alpha_x\alpha_y\beta_\parallel^2\left(\delta A_{x,m-2} - \delta A_{x,m+2}\right)\right] \ , \tag{13}$$

$$\Delta\omega_m\,\delta v_{z,m} + \frac{1}{2}\Omega_w\left(\delta v_{x,m-1} - \delta v_{x,m+1}\right) = -\frac{e}{\gamma_0\gamma_\parallel^2 m_e} k_m \delta\varphi_m$$

$$- \frac{e\beta_\parallel}{2\gamma_0 m_e c}\left(\alpha_x\left[\left(ck_{m-1} - \omega\beta_\parallel\right)\delta A_{x,m-1} + \left(ck_{m+1} - \omega\beta_\parallel\right)\delta A_{x,m+1}\right]\right.$$

$$\left. + \ i\,\alpha_y\left[\left(ck_{m-1} - \omega\beta_\parallel\right)\delta A_{y,m-1} - \left(ck_{m+1} - \omega\beta_\parallel\right)\delta A_{y,m+1}\right]\right) \ , \tag{14}$$

and

$$\Delta\omega_m\,\delta\gamma_m = -\frac{e}{m_e c^2}\left[k_m v_\parallel \delta\varphi_m - \frac{\omega}{2}\alpha_x\beta_\parallel\left(\delta A_{x,m-1} + \delta A_{x,m+1}\right)\right.$$

$$\left. + i\,\frac{\omega}{2}\alpha_y\beta_\parallel\left(\delta A_{y,m-1} - \delta A_{y,m+1}\right)\right] \ , \tag{15}$$

where $\Delta\omega_m \equiv \omega - k_m v_\parallel$,and $\beta_\parallel = v_\parallel/c$.

Examination of Eqs. (12) – (15) shows that the principal coupling is found between $\delta v_{z,m}$, $\delta\varphi_m$, $\delta v_{x,m\pm1}$, $\delta v_{y,m\pm1}$, $\delta A_{x,m\pm1}$, and $\delta A_{y,m\pm1}$. Retaining only these components, we find that after elimination of $\delta\gamma_m$ from these equations the transverse components of the perturbed velocity may be expressed in the form

$$\left(\Delta\omega_{m\pm1}^2 - \Omega_0^2\right)\delta v_{x,m\pm1} = \frac{e}{2\gamma_0\gamma_\parallel^2 m_e}\frac{k_m}{\Delta\omega_m}\delta\varphi_m\left[\alpha_x\beta_\parallel^2\gamma_\parallel^2\Delta\omega_{m\pm1}^2 \mp \alpha_y\Omega_0\left(\Phi_m\Delta\omega_{m\pm2} + \beta_\parallel^2\gamma_\parallel^2\Delta\omega_{m\pm1}\right)\right]$$

$$+\frac{e}{\gamma_0 m_e c}\delta A_{x,m\pm1}\left[\Delta\omega_{m\pm1}^2 - \frac{\alpha_x^2\beta_\parallel^2}{2}\frac{\omega\Delta\omega_{m\pm1}\left(\Delta\omega_{m\pm1}^2 + \Omega_0^2\right)}{\Delta\omega_m\Delta\omega_{m\pm2}} \pm \frac{\alpha_y\beta_\parallel}{4}\Omega_0\frac{\Delta\omega_{m\pm2}}{\Delta\omega_m}\left[\alpha_x\beta_\parallel\left(ck_{m\pm1} - \omega\beta_\parallel\right) - \Omega_w\Delta_m U_m^{(\pm)}\right]\right]$$

$$-\frac{ie}{\gamma_0 m_e c}\delta A_{y,m\pm1}\left[\Omega_0\Delta\omega_{m\pm1}\left(1 - \frac{\left(\alpha_x^2 + \alpha_y^2\right)}{2}\beta_\parallel^2\frac{\omega\Delta\omega_{m\pm1}}{\Delta\omega_m\Delta\omega_{m\pm2}}\right) - \frac{\alpha_y\beta_\parallel}{4}\Omega_0\frac{\Delta\omega_{m\pm2}}{\Delta\omega_m}\left[\alpha_y\beta_\parallel\left(ck_{m\pm1} - \omega\beta_\parallel\right) \mp \Omega_w\Delta_m V_m^{(\pm)}\right]\right]$$

$$-\frac{e}{4\gamma_0 m_e c}\delta A_{x,m\mp1}\left[\alpha_x\beta_\parallel^2\frac{\omega\Delta\omega_{m\pm1}}{\Delta\omega_m}\left(\alpha_x\Delta\omega_{m\pm1} \mp \alpha_y\Omega_0\right) \mp \alpha_y\Omega_0\frac{\Delta\omega_{m\pm2}}{\Delta\omega_m}\left[\alpha_x\beta_\parallel\left(ck_{m\mp1} - \omega\beta_\parallel\right) - \Omega_w\Delta_m U_m^{(\mp)}\right]\right]$$

$$\pm\frac{ie}{4\gamma_0 m_e c}\delta A_{y,m\mp1}\left[\alpha_y\beta_\parallel^2\frac{\omega\Delta\omega_{m\pm1}}{\Delta\omega_m}\left(\alpha_x\Delta\omega_{m\pm1} \mp \alpha_y\Omega_0\right) \mp \alpha_y\Omega_0\frac{\Delta\omega_{m\pm2}}{\Delta\omega_m}\left[\alpha_y\beta_\parallel\left(ck_{m\mp1} - \omega\beta_\parallel\right) \pm \Omega_w\Delta_m V_m^{(\mp)}\right]\right], \quad (16)$$

and

$$\left(\Delta\omega_{m\pm1}^2 - \Omega_0^2\right)\delta v_{y,m\pm1} = \mp\frac{ie}{2\gamma_0\gamma_\parallel^2 m_e}\frac{k_m}{\Delta\omega_m}\delta\varphi_m\left[\alpha_y\beta_\parallel^2\gamma_\parallel^2\Delta\omega_{m\pm1}\Delta\omega_{m\pm2} \mp \Phi_m\Omega_0\left(\alpha_x\Delta\omega_{m\pm1} \mp \alpha_y\Omega_0\right)\right]$$

$$+\frac{ie}{\gamma_0 m_e c}\delta A_{x,m\pm1}\left[\Omega_0\Delta\omega_{m\pm1}\left(1 - \alpha_x^2\beta_\parallel^2\frac{\omega\Delta\omega_{m\pm1}}{\Delta\omega_m\Delta\omega_{m\pm2}}\right) - \frac{\Omega_0}{4\Delta\omega_m}\left(\alpha_x\Delta\omega_{m\pm1} \mp \alpha_y\Omega_0\right)\left[\alpha_x\beta_\parallel\left(ck_{m\pm1} - \omega\beta_\parallel\right) - \Omega_w\Delta_m U_m^{(\pm)}\right]\right]$$

$$+\frac{e}{\gamma_0 m_e c}\,\delta A_{y,m\pm1}\left[\Delta\omega_{m\pm1}{}^2-\frac{\alpha_y{}^2\beta_{\|}{}^2}{2}\,\frac{\omega\,\Delta\omega_{m\pm1}\left(\Delta\omega_{m\pm1}{}^2+k_w{}^2 v_{\|}{}^2\right)}{\Delta\omega_m\,\Delta\omega_{m\pm2}}\right.$$
$$\left.\pm\frac{\Omega_0}{4\Delta\omega_m}\left(\alpha_x\Delta\omega_{m\pm1}\mp\alpha_y\Omega_0\right)\left[\alpha_y\beta_{\|}\left(ck_{m\pm1}-\omega\beta_{\|}\right)\mp\Omega_w\Delta_m V_m^{(\pm)}\right]\right]$$

$$\pm\frac{ie}{4\gamma_0 m_e c}\,\delta A_{x,m\mp1}\left[\alpha_x\alpha_y\beta_{\|}{}^2\frac{\omega\Delta\omega_{m\pm1}\Delta\omega_{m\pm2}}{\Delta\omega_m}\right.$$
$$\left.\mp\frac{\Omega_0}{\Delta\omega_m}\left(\alpha_x\Delta\omega_{m\pm1}\mp\alpha_y\Omega_0\right)\left[\alpha_x\beta_{\|}\left(ck_{m\mp1}-\omega\beta_{\|}\right)-\Omega_w\Delta_m U_m^{(\mp)}\right]\right]$$

$$+\frac{e}{4\gamma_0 m_e c}\,\delta A_{y,m\mp1}\left[\alpha_y{}^2\beta_{\|}{}^2\frac{\omega\Delta\omega_{m\pm1}\Delta\omega_{m\pm2}}{\Delta\omega_m}\right.$$
$$\left.\mp\frac{\Omega_0}{\Delta\omega_m}\left(\alpha_x\Delta\omega_{m\pm1}\mp\alpha_y\Omega_0\right)\left[\alpha_y\beta_{\|}\left(ck_{m\mp1}-\omega\beta_{\|}\right)\mp\Omega_w\Delta_m V_m^{(\mp)}\right]\right]\,, \qquad (17)$$

The axial component of the perturbed velocity is

$$\Delta\omega_m\delta v_{z,m}=-\frac{e}{\gamma_0\gamma_{\|}{}^2 m_e}\,k_m\Phi_m\,\delta\varphi_m$$
$$+\frac{e}{2\gamma_0 m_e c}\Big(\left[\alpha_x\beta_{\|}\left(ck_{m+1}-\omega\beta_{\|}\right)-\Omega_w\Delta_m U_m^{(+)}\right]\delta A_{x,m+1}$$
$$+\left[\alpha_x\beta_{\|}\left(ck_{m-1}-\omega\beta_{\|}\right)-\Omega_w\Delta_m U_m^{(-)}\right]\delta A_{x,m-1}$$
$$+i\left[\alpha_y\beta_{\|}\left(ck_{m+1}-\omega\beta_{\|}\right)-\Omega_w\Delta_m V_m^{(+)}\right]\delta A_{y,m+1}$$
$$-i\left[\alpha_y\beta_{\|}\left(ck_{m-1}-\omega\beta_{\|}\right)+\Omega_w\Delta_m V_m^{(-)}\right]\delta A_{y,m-1}\Big)\,, \qquad (18)$$

The coefficients which appear in Eq. (18) are defined as

$$\Phi_m\equiv 1-\frac{\gamma_{\|}{}^2\alpha_y\Omega_0\Omega_w\left(\Omega_0{}^2+3k_w{}^2 v_{\|}{}^2-\Delta\omega_m{}^2\right)}{2\left(\Delta\omega_{m+1}{}^2-\Omega_0{}^2\right)\left(\Delta\omega_{m-1}{}^2-\Omega_0{}^2\right)+\alpha_y\Omega_0\Omega_w\left(\Omega_0{}^2+3k_w{}^2 v_{\|}{}^2-\Delta\omega_m{}^2\right)}\,, \qquad (19)$$

$$U_m^{(\pm)}\equiv\mp\frac{\Delta\omega_{m\pm1}}{\Delta\omega_{m\pm1}{}^2-\Omega_0{}^2}\left[\Delta\omega_{m\pm1}-\frac{\alpha_x{}^2\beta_{\|}{}^2}{2}\,\frac{\omega\left(\Delta\omega_{m\pm1}{}^2+\Omega_0{}^2\right)}{\Delta\omega_m\,\Delta\omega_{m\pm2}}\right]$$
$$\mp\frac{\alpha_x\beta_{\|}{}^2}{4}\,\frac{\omega\,\Delta\omega_{m\mp1}}{\Delta\omega_m}\,\frac{\alpha_x\Delta\omega_{m\mp1}\pm\alpha_y\Omega_0}{\left(\Delta\omega_{m\mp1}{}^2-\Omega_0{}^2\right)}$$

$$+ \frac{\alpha_x \beta_\parallel}{2}\left(ck_{m\pm1} - \omega\beta_\parallel\right)\frac{\alpha_y\Omega_0\left(\Omega_0^{\,2} + 3k_w^{\,2}v_\parallel^{\,2} - \Delta\omega_m^{\,2}\right)}{\left(\Delta\omega_{m+1}^{\,2} - \Omega_0^{\,2}\right)\left(\Delta\omega_{m-1}^{\,2} - \Omega_0^{\,2}\right)} , \quad (20)$$

$$V_m^{(\pm)} \equiv \pm\frac{\Omega_0\Delta\omega_{m\pm1}}{\Delta\omega_{m\pm1}^{\,2} - \Omega_0^{\,2}}\left[1 - \frac{\left(\alpha_x^{\,2} + \alpha_y^{\,2}\right)}{2}\beta_\parallel^{\,2}\frac{\omega\,\Delta\omega_{m\pm1}}{\Delta\omega_m\,\Delta\omega_{m\pm2}}\right]$$

$$- \frac{\alpha_y\beta_\parallel^{\,2}}{4}\frac{\omega\,\Delta\omega_{m\mp1}}{\Delta\omega_m}\frac{\alpha_x\Delta\omega_{m\mp1} \pm \alpha_y\Omega_0}{\left(\Delta\omega_{m\mp1}^{\,2} - \Omega_0^{\,2}\right)}$$

$$\pm \frac{\alpha_y\beta_\parallel}{2}\left(ck_{m\pm1} - \omega\beta_\parallel\right)\frac{\alpha_y\Omega_0\left(\Omega_0^{\,2} + 3k_w^{\,2}v_\parallel^{\,2} - \Delta\omega_m^{\,2}\right)}{\left(\Delta\omega_{m+1}^{\,2} - \Omega_0^{\,2}\right)\left(\Delta\omega_{m-1}^{\,2} - \Omega_0^{\,2}\right)} , \quad (21)$$

and

$$\Delta_m \equiv \frac{2\left(\Delta\omega_{m+1}^{\,2} - \Omega_0^{\,2}\right)\left(\Delta\omega_{m-1}^{\,2} - \Omega_0^{\,2}\right)}{2\left(\Delta\omega_{m+1}^{\,2} - \Omega_0^{\,2}\right)\left(\Delta\omega_{m-1}^{\,2} - \Omega_0^{\,2}\right) + \alpha_y\Omega_0\Omega_w\left(\Omega_0^{\,2} + 3k_w^{\,2}v_\parallel^{\,2} - \Delta\omega_m^{\,2}\right)} . \quad (22)$$

Note that $\Phi_m \to \Phi$ in the limit as $\Delta\omega_m \to 0$.

The source currents may be expressed in terms of the solutions for the perturbed charge density and velocities, and we find that

$$\delta\mathbf{J}_{\perp,m\pm1} = -en_0\left[\delta\mathbf{v}_{\perp,m\pm1} + \frac{1}{2}\left(\alpha_x\hat{\mathbf{e}}_x \mp \alpha_y\hat{\mathbf{e}}_y\right)\frac{k_m v_\parallel}{\Delta\omega_m}\delta v_{z,m}\right] . \quad (23)$$

The dispersion equations are obtained by substitution of the source currents and charge density into the Maxwell-Poisson equations

$$\left(\frac{\omega^2}{c^2} - k_{m\pm1}^2\right)\delta\mathbf{A}_{\perp,m\pm1} = -\frac{4\pi}{c}\delta\mathbf{J}_{\perp,m\pm1} , \quad (24)$$

and

$$k_m^2\,\delta\varphi_m = 4\pi e\,\delta n_m . \quad (25)$$

IV. LINEAR STABILITY THEORY: $\mathbf{B}_0 = 0$

Substantial simplifications in the source current and charge density occur in the absence of an axial guide field. In this limit, the interaction is with plane-polarized waves and the y-component of the fields and velocities vanishes. The x- and z-components of the velocities can be expressed as

$$\delta v_{x,m\pm1} = -\frac{e}{2\gamma_0 m_e c}\left(\frac{\Omega_w}{ck_w}\right)\frac{k_m v_{\parallel}}{\Delta\omega_m}\,\delta\varphi_m + \frac{e}{\gamma_0 m_e c}\,\delta A_{x,m\pm1}\left[1-\left(\frac{\Omega_w}{ck_w}\right)^2\frac{\omega\,\Delta\omega_{m\pm1}}{2\Delta\omega_m\,\Delta\omega_{m\pm2}}\right], \quad (26)$$

and

$$\Delta\omega_m\delta v_{z,m} = -\frac{e}{\gamma_0\gamma_{\parallel}^2 m_e}\,k_m\,\delta\varphi_m - \frac{e}{2\gamma_0 m_e c}\left(\frac{\Omega_w}{ck_w}\right)\left(ck_m-\omega\beta_{\parallel}\right)\left(\delta A_{x,m+1}+\delta A_{x,m-1}\right), \quad (27)$$

where only the lowest order couplings have been retained. Substitution of Eq. (27) into Poisson's equation now yields

$$\left(\Delta\omega_m^2-\frac{\omega_b^2}{\gamma_{\parallel}^2}\right)\delta\varphi_m = \frac{1}{2}\frac{\omega_b^2}{ck_m}\left(\frac{\Omega_w}{ck_w}\right)\left(ck_m-\omega\beta_{\parallel}\right)\left[\delta A_{x,m+1}+\delta A_{x,m-1}\right], \quad (28)$$

where $\omega_b^2 \equiv 4\pi e^2 n_0/\gamma_0 m_e$. The substitution of Eq. (26) into Maxwell's equation yields

$$\left[\omega^2-c^2k_{m\pm1}^2-\omega_b^2\left(1-\frac{\Omega_w^2}{4c^2k_w^2}\frac{\omega^2-c^2k_m^2}{\Delta\omega_m^2}\right)\right]\delta A_{x,m\pm1} = -\frac{\omega_b^2}{2\gamma_{\parallel}^2}\frac{\Omega_w}{ck_w}\frac{ck_m}{\Delta\omega_m}\left(\beta_{\parallel}\gamma_{\parallel}^2-\frac{ck_m}{\Delta\omega_m}\right)\delta\varphi_m . \quad (29)$$

The FEL Doppler upshift principally deals with a coupling between $\delta\varphi_m$ and $\delta A_{x,m-1}$. Hence, we neglect the terms in $\delta A_{x,m+1}$ and set the determinant of the resulting system of equations to zero, then we obtain the well-known cold-beam dispersion equation

$$\left(\Delta\omega_m^2-\frac{\omega_b^2}{\gamma_{\parallel}^2}\right)\left(\omega^2-c^2k_{m-1}^2-\omega_b^2\right) = -\frac{\omega_b^2}{4}\left(\frac{\Omega_w}{ck_w}\right)^2\left(\omega^2-c^2k_m^2-\omega_b^2\right). \quad (30)$$

This dispersion equation reduces to both the Raman and strong-pump Compton[18] regimes in the appropriate limits, and is identical to the dispersion equation obtained for a helical wiggler field under the substitution $B_w^2 \rightarrow 2B_w^2$. The reason for this substitution is that the *average* transverse wiggler velocity for a planar wiggler is determined by the root-mean-square of the wiggler field. A second difference between the results for planar and helical wigglers is the polarization of the amplified signal, which is linear for the planar and circular for the helical wiggler. As we shall discuss in the following section, such a close correspondence between the results for planar and helical wigglers is not found in the presence of an axial guide field. This is due to the fact that the normal modes of a uniformly magnetized plasma are circularly polarized while the orbits in a combined planar wiggler/axial guide field are elliptic. As a result, in contrast to the case of a helical wiggler, both the right- and left-hand circularly polarized modes are amplified.

V. LINEAR STABILITY THEORY : $B_0 \neq 0$

Since the presence of an axial guide field means that the normal modes of the system (in the absence of the wiggler field) are circularly polarized, we transform to a circularly polarized basis in which $\delta A_m^{(\pm)} \equiv \delta A_{x,m} \mp i\, \delta A_{y,m}$. Substitution of the source currents into Maxwell's equations in this representation yields

$$\left[\omega^2 - c^2 k_{m\pm1}{}^2 - \omega_b{}^2 \left(\frac{\Delta\omega_{m\pm1}}{\Delta\omega_{m\pm1} - \Omega_0} - \frac{1}{8}(\alpha_x \mp \alpha_y)^2 \Lambda^{(+)}_{m,m\pm1}\right)\right] \delta A^{(+)}_{m\pm1} =$$

$$= \frac{\omega_b{}^2 (\alpha_x \mp \alpha_y)}{2\gamma_\parallel{}^2} \frac{ck_m}{\Delta\omega_m} \delta\varphi_m \left[\frac{\beta_\parallel{}^2 \gamma_\parallel{}^2 \Delta\omega_{m\pm1} + \Phi_m \Omega_0}{\Delta\omega_{m\pm1} - \Omega_0} - \Phi_m \frac{k_m v_\parallel}{\Delta\omega_m}\right], \quad (31)$$

and

$$\left[\omega^2 - c^2 k_{m\pm1}{}^2 - \omega_b{}^2 \left(\frac{\Delta\omega_{m\pm1}}{\Delta\omega_{m\pm1} + \Omega_0} - \frac{1}{8}(\alpha_x \pm \alpha_y)^2 \Lambda^{(-)}_{m,m\pm1}\right)\right] \delta A^{(-)}_{m\pm1} =$$

$$= \frac{\omega_b{}^2 (\alpha_x \pm \alpha_y)}{2\gamma_\parallel{}^2} \frac{ck_m}{\Delta\omega_m} \delta\varphi_m \left[\frac{\beta_\parallel{}^2 \gamma_\parallel{}^2 \Delta\omega_{m\pm1} - \Phi_m \Omega_0}{\Delta\omega_{m\pm1} + \Omega_0} - \Phi_m \frac{k_m v_\parallel}{\Delta\omega_m}\right], \quad (32)$$

while Poisson's equation becomes

$$\left(\Delta\omega_m{}^2 - \frac{\omega_b{}^2}{\gamma_\parallel{}^2}\Phi_m\right)\delta\varphi_m = -\frac{\omega_b{}^2}{4ck_m}\left(k_m v_\parallel - \omega\beta_\parallel{}^2\right)\Psi_m\left[(\alpha_x - \alpha_y)\left(\delta A^{(+)}_{m+1} + \delta A^{(-)}_{m-1}\right)\right.$$

$$\left. + (\alpha_x + \alpha_y)\left(\delta A^{(-)}_{m+1} + \delta A^{(+)}_{m-1}\right)\right]. \quad (33)$$

In Eqs. (31) – (33), we have defined

$$\Lambda^{(\pm)}_{l,m} \equiv \beta_\parallel{}^2 \frac{\omega\Delta\omega_m}{\Delta\omega_l\left(\Delta\omega_m \mp \Omega_0\right)} - \Psi_l\left(k_l v_\parallel - \omega\beta_\parallel{}^2\right)\left(\frac{k_l v_\parallel}{\Delta\omega_l} \mp \frac{\Omega_0}{\left(\Delta\omega_m \mp \Omega_0\right)}\right), \quad (34)$$

and

$$\Psi_m \equiv 1 - \frac{\alpha_y \Omega_0 \Omega_w \left(\Omega_0{}^2 + 3k_w{}^2 v_\parallel{}^2 - \Delta\omega_m{}^2\right)}{2\left(\Delta\omega_{m+1}{}^2 - \Omega_0{}^2\right)\left(\Delta\omega_{m-1}{}^2 - \Omega_0{}^2\right) + \alpha_y \Omega_0 \Omega_w \left(\Omega_0{}^2 + 3k_w{}^2 v_\parallel{}^2 - \Delta\omega_m{}^2\right)}, \quad (35)$$

The principal coupling, as in the absence of the guide field, occurs between $\delta\varphi_m$ and $\delta A_{m-1}{}^{(\pm)}$ which reflects the parametric interaction between the radiation field and a space-charge wave up-shifted by one unit of k_w in the wavelength. Retaining only this

dominant coupling, we obtain the dispersion equations for the right- and left-hand modes by setting the determinant of the resulting equations to zero. In the limit of a tenuous beam (i.e., $\omega_b << ck_w$), this gives

$$\left(\Delta\omega_m^2 - \frac{\omega_b^2}{\gamma_\parallel^2}\Phi\right)\left(\omega^2 - ck_{m-1}^2 - \frac{\omega_b^2\Delta\omega_{m-1}}{\Delta\omega_{m-1} \mp \Omega_0}\right) = \frac{\omega_b^2\Omega_w\Psi}{4\left(\Omega_0 \mp k_w v_\parallel\right)^2} k_{m-1}k_w v_\parallel^2, \qquad (36)$$

where the resonance condition given by $\Delta\omega_m \approx 0$ has been implicitly imposed in the source terms, and

$$\Psi \equiv 1 - \frac{\alpha_y^2\left(\Omega_0^2 + 3k_w^2v_\parallel^2\right)}{2\left(\Omega_0^2 - k_w^2v_\parallel^2\right) + \alpha_y^2\left(\Omega_0^2 + 3k_w^2v_\parallel^2\right)}. \qquad (37)$$

This is similar to the result found for a helical wiggler field, except that the left-hand polarization is also excited. Observe that in the limit as $B_0 \to 0$ the dispersion equations for both the right- and left-hand modes are identical, which indicates that the amplified wave is linearly polarized.

We now solve the dispersion equation (36) for Group I trajectories. The growth rate Im k/k_w is shown in Fig. 3 and 4 as a function of frequency for a 1 MeV beam kinetic energy, $\omega_b/ck_w = 0.1$, $\Omega_w/\sqrt{2}ck_w = 0.05$, and a variety of axial field strengths corresponding to the right-hand circularly polarized (RHCP) and left-hand circularly polarized (LHCP) modes. It should be noted that for both the RHCP and LHCP modes the interaction is with an escape mode of the plasma. It is evident from the figure that the peak growth increases with increasing guide field for the RHCP mode corresponding to the approach to the resonance at $\Omega_0 \approx k_w v_\parallel$. Since the axial velocity decreases with the increase in the transverse velocity near resonance, the interaction frequency must decrease as well. This contrasts with the behavior of the LHCP mode in which it is seen that the growth rate decreases and the interaction frequency increases as the resonance is approached. Note that the growth rates of the two modes are identical in the limit of a vanishing axial guide field in which the interaction is with a linearly polarized wave. As the magnetic resonance is approached, however, the polarization of the wave becomes increasing circular, and this accounts for the decrease in the growth rate of the LHCP mode.

Turning to the case of Group II orbits for $\Phi > 0$, we observe that the RHCP mode can interact only on the cyclotron branch of the dispersion curve, which is in accord with the interaction for a helical wiggler.[4] The growth rate for this mode is shown in Fig. 5 as a function of frequency for $\Omega_0/ck_w = 1.2$ and 1.4. The transverse wiggler-induced velocity decreases with increasing axial fields while Φ is bounded by unity in this regime, and both the coupling coefficients and the growth rate decreases as a result. However, the decrease in the transverse velocity gives rise to an increase in the interaction frequency with B_0. Similar behavior is found for the LHCP mode (escape branch) in this regime, as shown in Fig. 6.

A summary of the behavior of the instability when $\Phi > 0$ is shown in Fig. 7, in which we plot (a) the maximum growth rates and (b) the frequencies corresponding to maximum growth of the RHCP and LHCP modes as a function of the axial guide field. The general increase in the growth rate and decrease in the interaction frequency near the resonance at $\Omega_0 \approx k_w v_\parallel$ is apparent. The decrease in the growth rate of the LHCP mode

near the resonance is also shown, and arises due to the increasingly circular polarization of the electron trajectories.

When $\Phi < 0$ for the Group II orbits, the interaction is with the RHCP cyclotron mode. There is no direct intersection between the LHCP mode and the beam resonance line; however, the unstable space-charge wave can give rise to instability. In both cases, the instability is extremely broad-band in nature. An example of this regime is shown in Fig. 8, in which we plot the growth rates of the RHCP and LHCP modes versus frequency for $\Omega_0/ck_w = 1.0$ corresponding to $\Phi = -1.51$. The growth rate of the LHCP mode is equal to the growth rate of the space-charge mode, that is

$$\mathrm{Im}\,\frac{k}{k_w} = \frac{\omega_b}{\gamma_{\|} c k_w} |\Phi| \ , \tag{38}$$

and is independent of frequency. The growth rate of the RHCP mode displays some structure near the frequency where the beam resonance line and the cyclotron branch intersect, but approaches this value asymptotically at high frequencies, .

IV. SUMMARY AND DISCUSSION

In this paper we have analyzed the linear growth rate in both the Compton and collective regimes of a Free-Electron Laser configuration which contains a planar wiggler and an axial guide field. The technique employed is that of a cold fluid model of the perturbations about the single-particle trajectories, and includes the effects of stimulated Raman scattering by the beam space-charge modes as well as the ponderomotive effect of the wiggler itself.

The results have shown many similarities with the linear theory of the helical wiggler FEL. In particular, the transverse velocity and the linear growth rate both increase as the axial field approaches the value at which the Larmor period coincides with the wiggler period. In addition, a negative-mass regime is found in which the axial electron velocity increases as the beam loses energy. This axial acceleration is accompanied by an enhanced deceleration in the transverse direction, and corresponds to an instability in the beam space-charge modes. The principal distinction with the helical wiggler configuration lies in the polarization of the amplified signal. In the case of the helical wiggler, the projection of the electron trajectories on the transverse plane is circular, and the interaction is with an RHCP mode. By contrast, the projections of the electron trajectories in the transverse plane for a planar wiggler configuration are ellipses. As a result, the amplified signal in a planar wiggler/axial guide field configuration is elliptically polarized.

ACKNOWLEDGEMENTS

This work has been supported in part by the Office of Naval Research, in part by the National Science Foundation, and in part by the Naval Research Laboratory Plasma Physics Division..

REFERENCES

1. T. Kwan and J.M. Dawson, Phys. Fluids **22**, 1089 (1979).
2. R.C. Davidson and H.S. Uhm, Phys. Fluids **23**, 2076 (1980).
3. I.B. Bernstein and L. Friedland, Phys. Rev. A **23**, 816 (1981).
4. H.P. Freund, P. Sprangle, D. Dillenburg, E.H. da Jornada, R.S. Schneider, and B. Liberman, Phys. Rev. A **26**, 2004 (1982).
5. L. Friedland and A. Fruchtman, Phys. Rev. A **25**, 2693 (1982).
6. H.P. Freund, Phys. Rev. A **27**, 1977 (1983).
7. H.S. Uhm and R.C. Davidson, Phys. Fluids **24**, 1541 (1981).
8. H.S. Uhm and R.C. Davidson, Phys. Fluids **24**, 2348 (1981).
9. H.P. Freund and A.K. Ganguly, Phys. Rev. A **28**, 3438 (1983).
10. A.K. Ganguly and H.P. Freund, Phys. Rev. A **32**, 2275 (1985).
11. J. Fajans, G. Bekefi, Y.Z. Yin, and B. Lax, Phys. Fluids **28**, 1995 (1985).
12. J. Masud, T.C. Marshall, S.P. Schlesinger, and F.G. Yee, Phys. Rev. Lett. **56**, 1567 (1986).
13. D.A. Kirkpatrick, G. Bekefi, A.C. DiRienzo, H.P. Freund, and A.K. Ganguly, Phys. Fluids (submitted for publication).
14. K.D. Jacobs, Ph.D. dissertation (MIT, 1986).
15. L. Friedland, Phys. Fluids **23**, 2376 (1980).
16. H.P. Freund and A.T. Drobot, Phys. Fluids **25**, 736 (1982).
17. H.P. Freund and P. Sprangle, Phys. Rev. A **28**, 1835 (1983).
18. R.C. Davidson and J.S. Wurtele, IEEE Trans. Plasma Sci. **PS-13**, 464 (1985); R.C. Davidson, Phys. Fluids **29**, 267 (1986).

FIGURE CAPTIONS

Fig. 1 The positive branch of the solutions for the axial velocity as a function of the axial magnetic field.

Fig. 2 A graph of the function Φ corresponding to both Group I and II orbits for the parameters used in Fig. 1.

Fig. 3 Graph of the growth rate as a function of frequency for the RHCP mode (escape branch) and Group I electron trajectories.

Fig. 4 Graph of the growth rate as a function of frequency for the LHCP mode (cyclotron branch) and Group I electron trajectories.

Fig. 5 Graph of the growth rate of the RHCP mode (cyclotron branch) as a function of frequency for Group II orbits when $\Phi > 0$.

Fig. 6 Graph of the growth rate of the LHCP mode (escape branch) as a function of frequency for Group II orbits when $\Phi > 0$.

Fig. 7 Plots of (a) the frequency corresponding to peak growth, and (b) the peak growth rate as a function of the axial magnetic field.

Fig. 8 Graph of the growth rates of both the RHCP and LHCP modes as a function of frequency for Group II orbits corresponding to $\Phi < 0$.

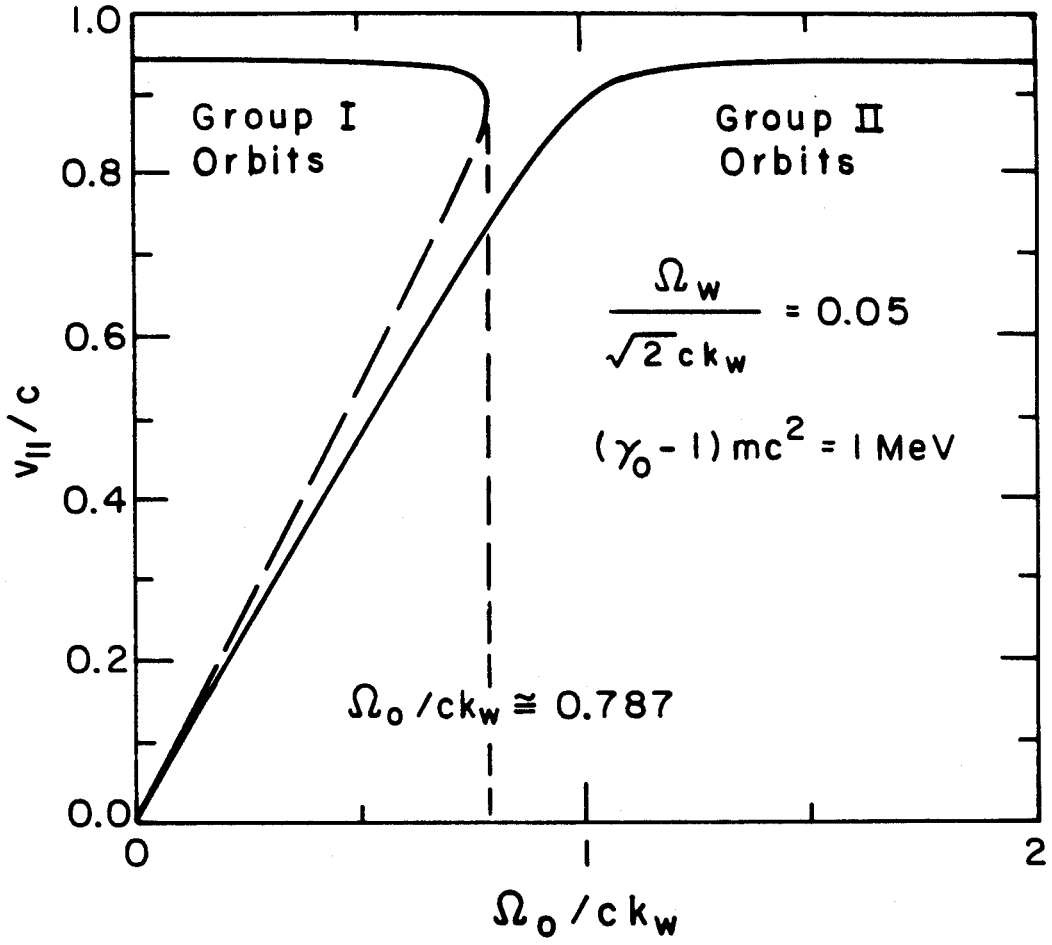
1.0
0.8
0.6
0.4
0.2
0.0
0
2
$v_{\parallel}/c$
Ω_0/ck_w
Group I
Orbits
Group II
Orbits
$\frac{\Omega_w}{\sqrt{2}ck_w} = 0.05$
$(\gamma_0 - 1)mc^2 = 1\,MeV$
$\Omega_0/ck_w \cong 0.787$

Fig. 1

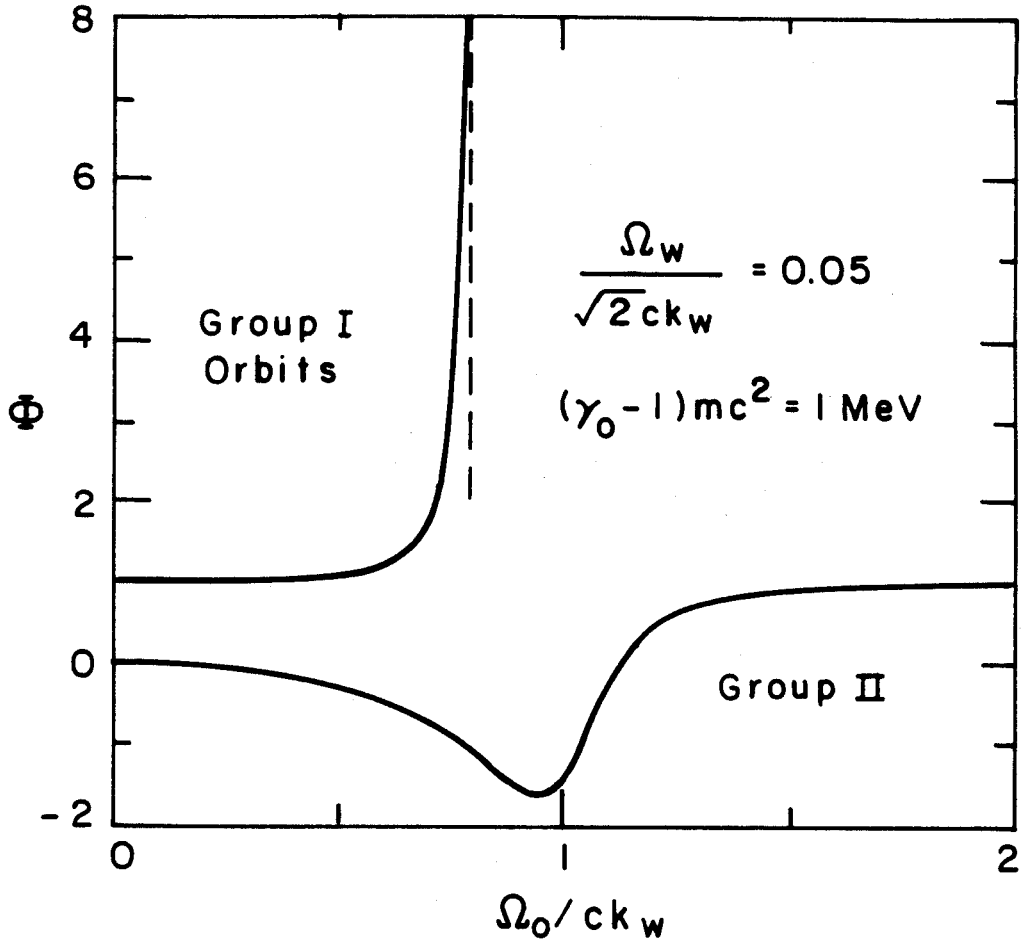
8
6
4
2
0
-2
Φ
0
1
2
Ω_0 / ck_w
Group I
Orbits
$\frac{\Omega_w}{\sqrt{2}ck_w} = 0.05$
$(\gamma_0 - 1)mc^2 = 1\ MeV$
Group II

Fig. 2

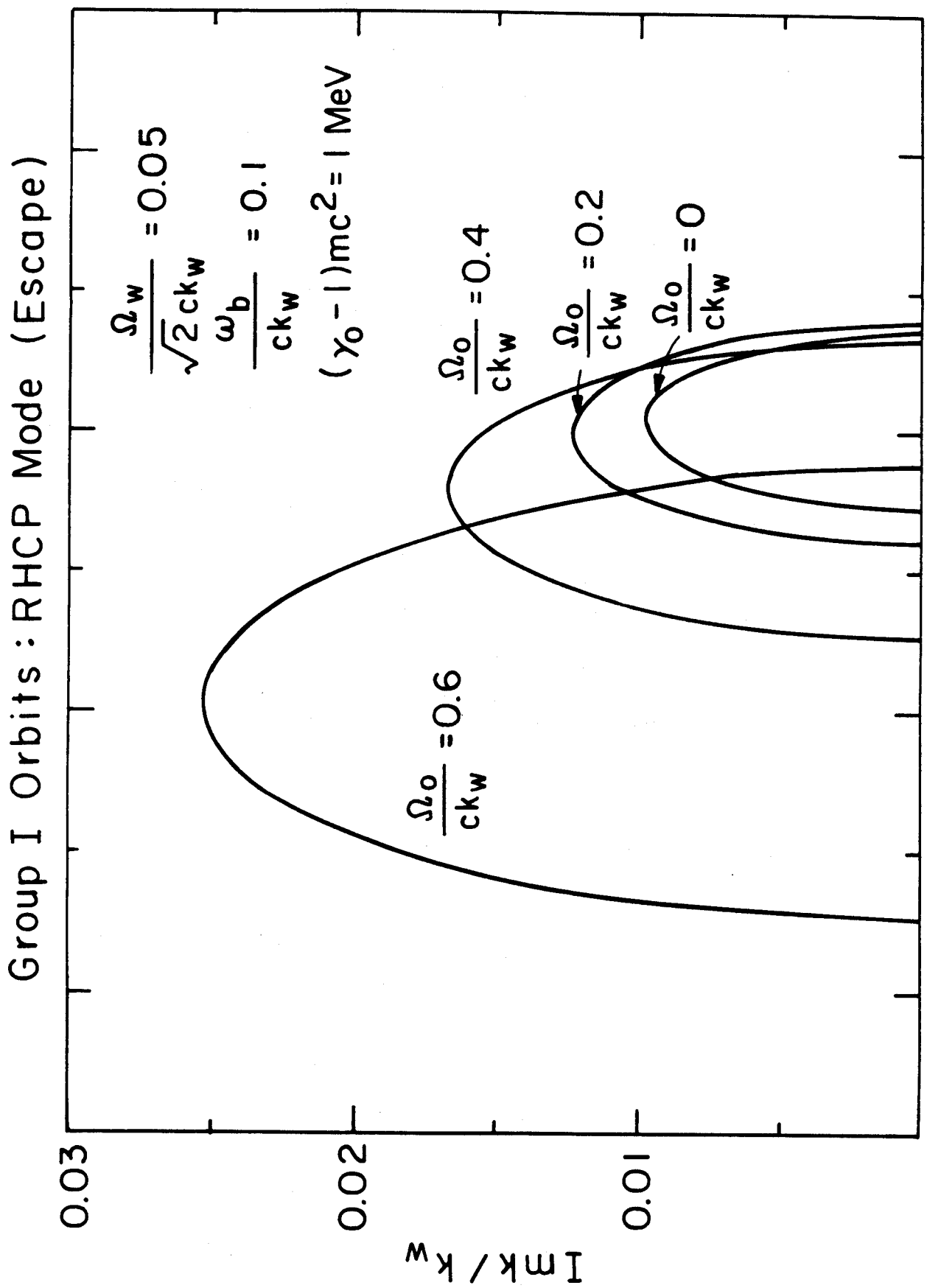
Group I Orbits : RHCP Mode (Escape)
$\frac{\Omega_w}{\sqrt{2}ck_w} = 0.05$
$\frac{\omega_b}{ck_w} = 0.1$
$(\gamma_0 - 1)mc^2 = 1$ MeV
$\frac{\Omega_o}{ck_w} = 0.4$
$\frac{\Omega_o}{ck_w} = 0.2$
$\frac{\Omega_o}{ck_w} = 0$
$\frac{\Omega_o}{ck_w} = 0.6$
0.03
0.02
0.01
$\mathrm{Im}k / k_w$
13
14
15
16
ω / ck_w

Fig. 3

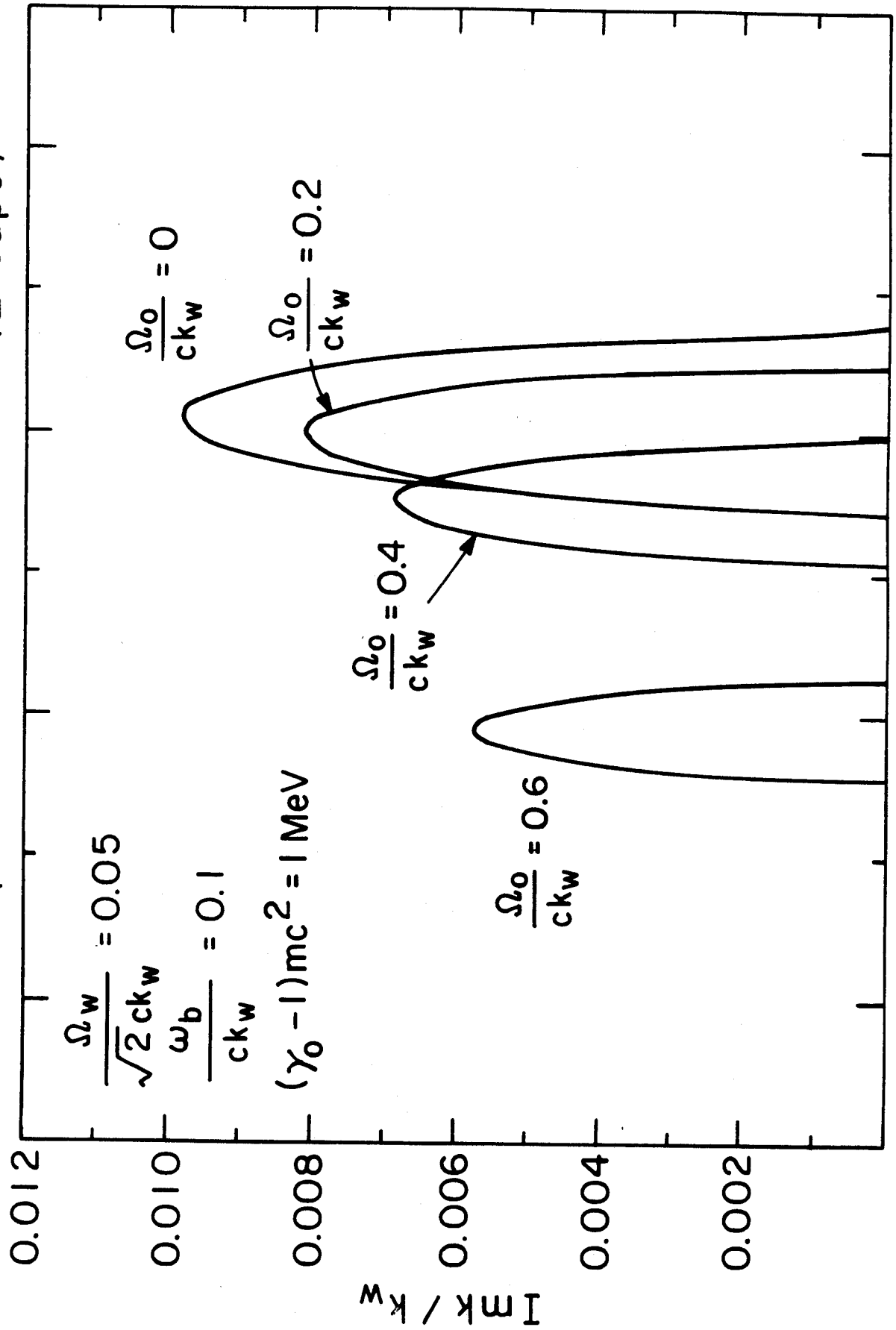
Group I Orbits : LHCP Mode (Escape)
$\frac{\Omega_w}{\sqrt{2}ck_w} = 0.05$
$\frac{\omega_b}{ck_w} = 0.1$
$(\gamma_0 - 1)mc^2 = 1\,MeV$
$\frac{\Omega_o}{ck_w} = 0$
$\frac{\Omega_o}{ck_w} = 0.2$
$\frac{\Omega_o}{ck_w} = 0.4$
$\frac{\Omega_o}{ck_w} = 0.6$
$\Im k / k_w$
ω / ck_w
0.012
0.010
0.008
0.006
0.004
0.002
13
14
15
16

Fig. 4

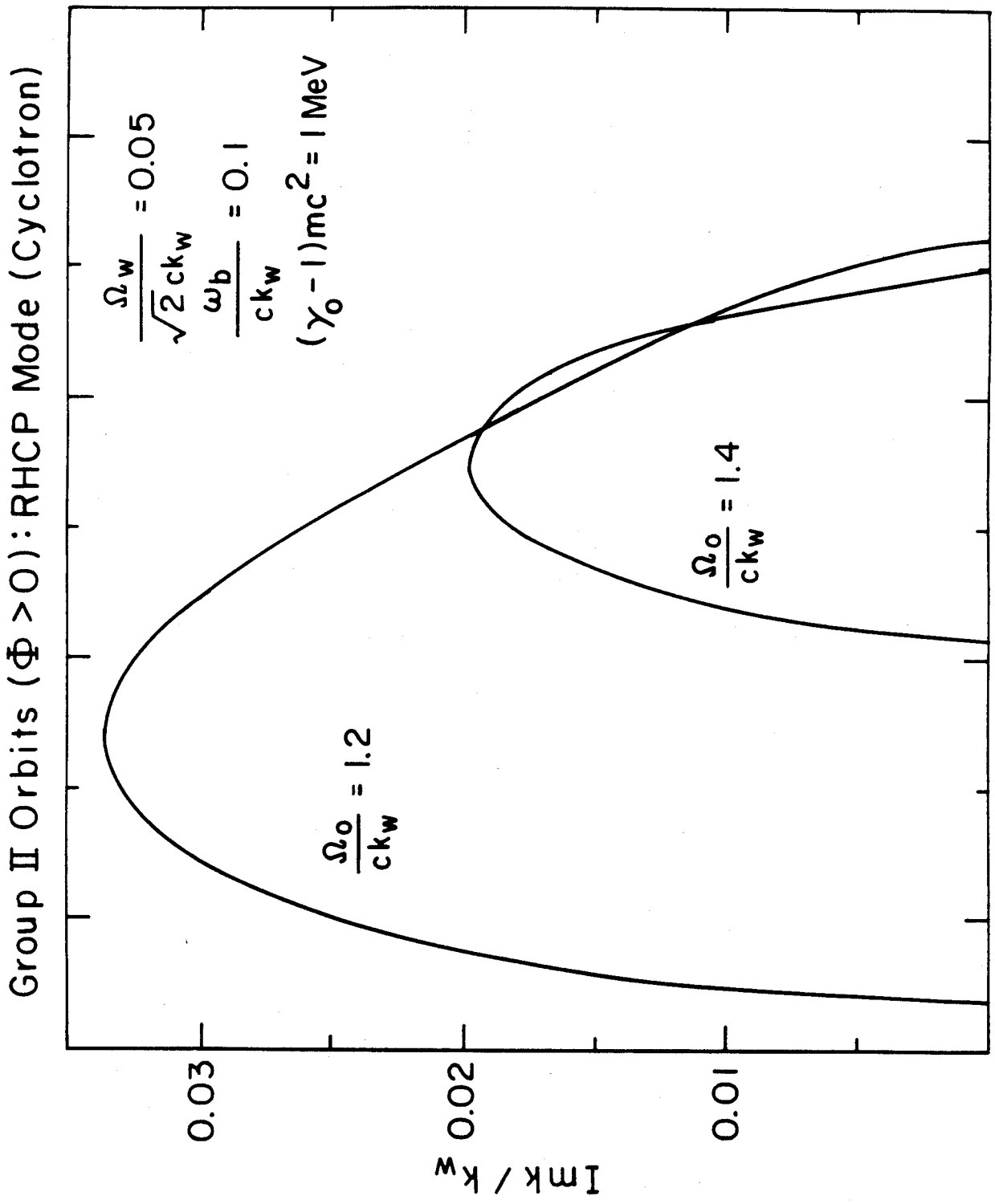
Group II Orbits ($\Phi > 0$): RHCP Mode (Cyclotron)
$\frac{\Omega_w}{\sqrt{2}ck_w} = 0.05$
$\frac{\omega_b}{ck_w} = 0.1$
$(\gamma_o - 1)mc^2 = 1$ MeV
$\frac{\Omega_o}{ck_w} = 1.2$
$\frac{\Omega_o}{ck_w} = 1.4$
Imk / k_w
0.03
0.02
0.01
13
14
15
16
ω / ck_w

Fig. 5

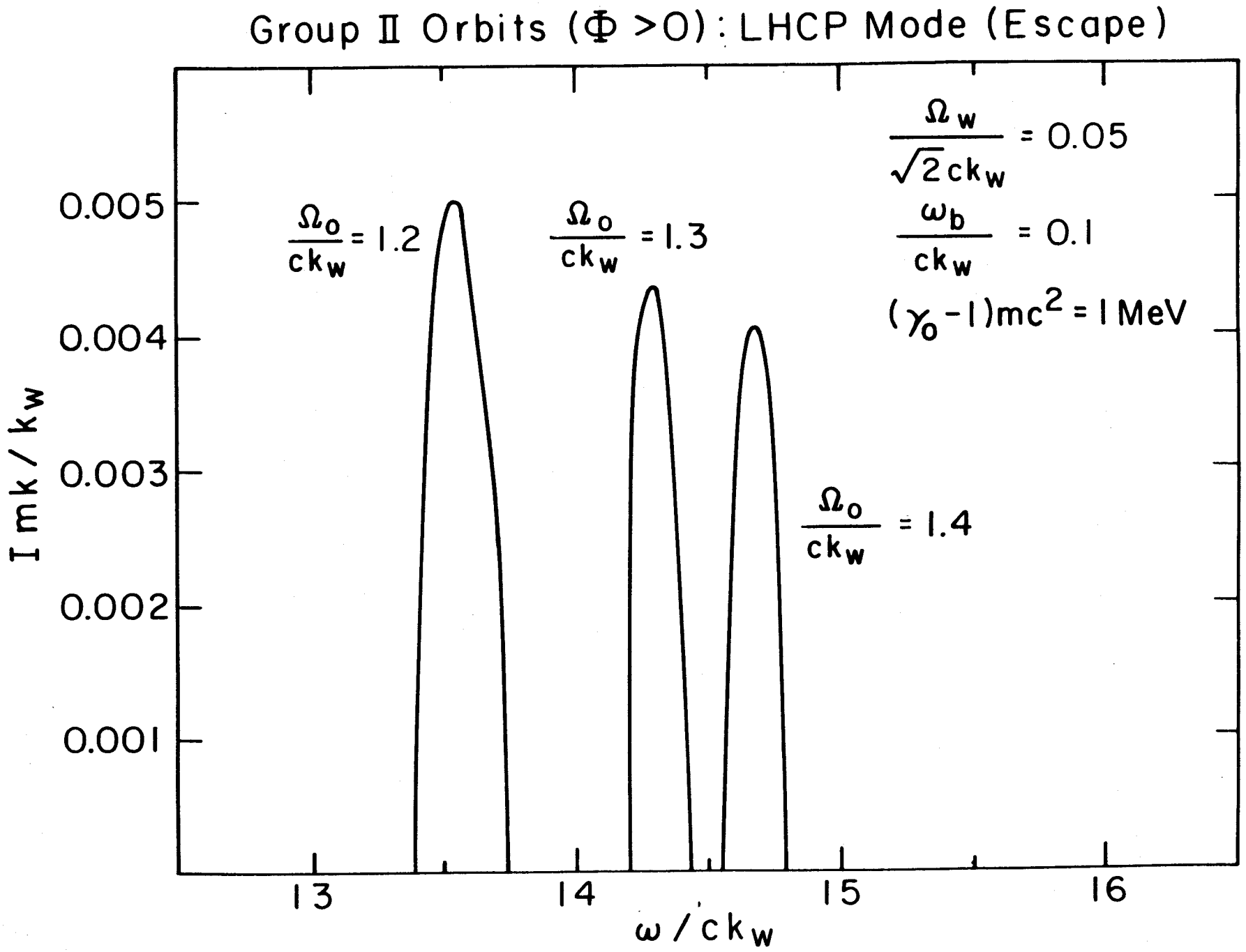
Group II Orbits (Φ >0) : LHCP Mode (Escape)
$\frac{\Omega_w}{\sqrt{2}ck_w} = 0.05$
$\frac{\omega_b}{ck_w} = 0.1$
$(\gamma_0 - 1)mc^2 = 1\,MeV$
$\frac{\Omega_0}{ck_w} = 1.2$
$\frac{\Omega_0}{ck_w} = 1.3$
$\frac{\Omega_0}{ck_w} = 1.4$
0.005
0.004
0.003
0.002
0.001
Imk / k_w
13
14
15
16
ω / ck_w

Fig. 6

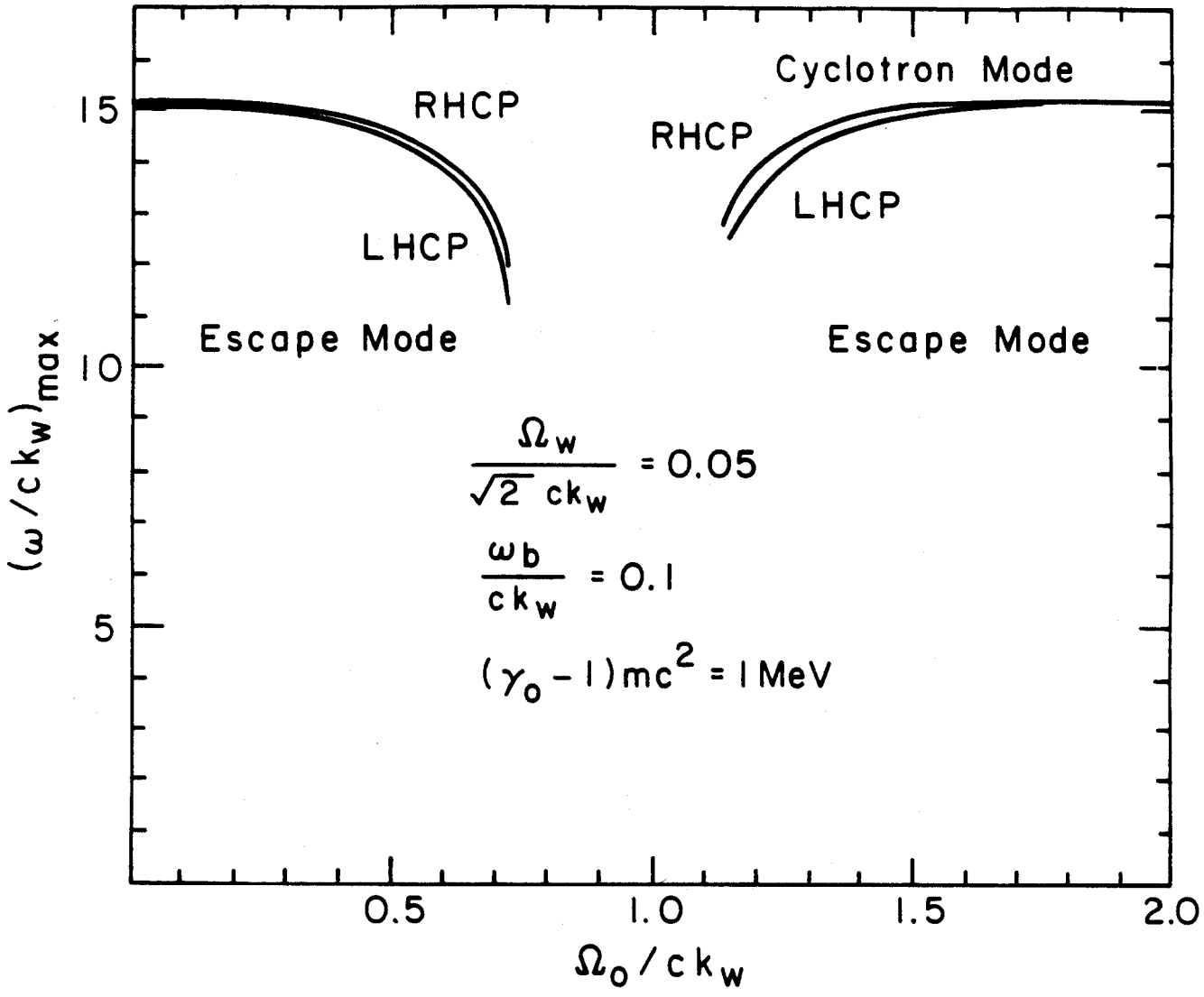
Cyclotron Mode
RHCP
RHCP
LHCP
LHCP
Escape Mode
Escape Mode
$\frac{\Omega_w}{\sqrt{2}\,ck_w} = 0.05$
$\frac{\omega_b}{ck_w} = 0.1$
$(\gamma_0 - 1)mc^2 = 1\,MeV$
15
10
5
$(\omega/ck_w)_{max}$
0.5
1.0
1.5
2.0
Ω_0/ck_w

Fig. 7(a)

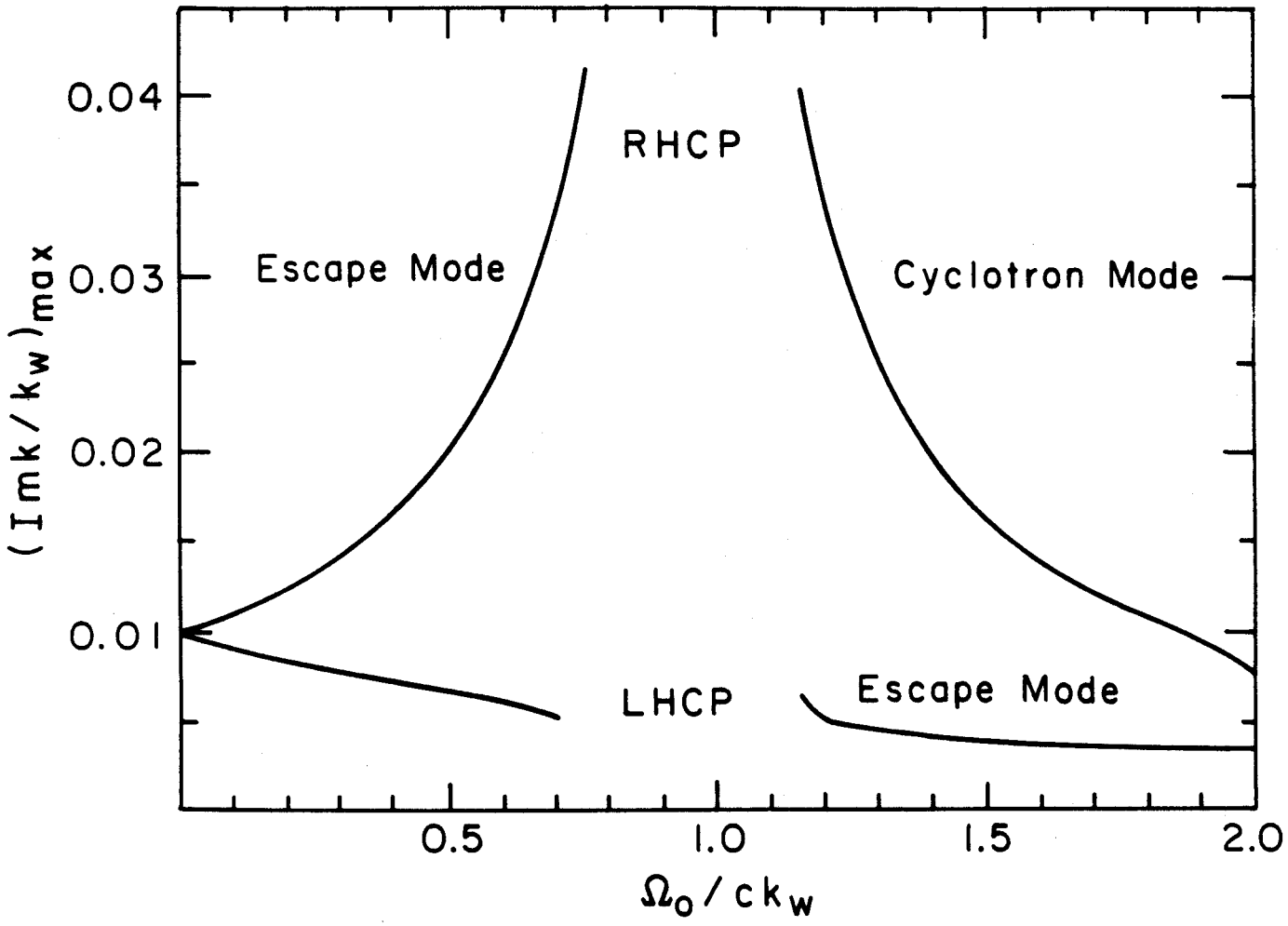
0.04
0.03
0.02
0.01
$(Imk/k_w)_{max}$
RHCP
Escape Mode
Cyclotron Mode
LHCP
Escape Mode
0.5
1.0
1.5
2.0
Ω_o / ck_w

Fig. 7(b)

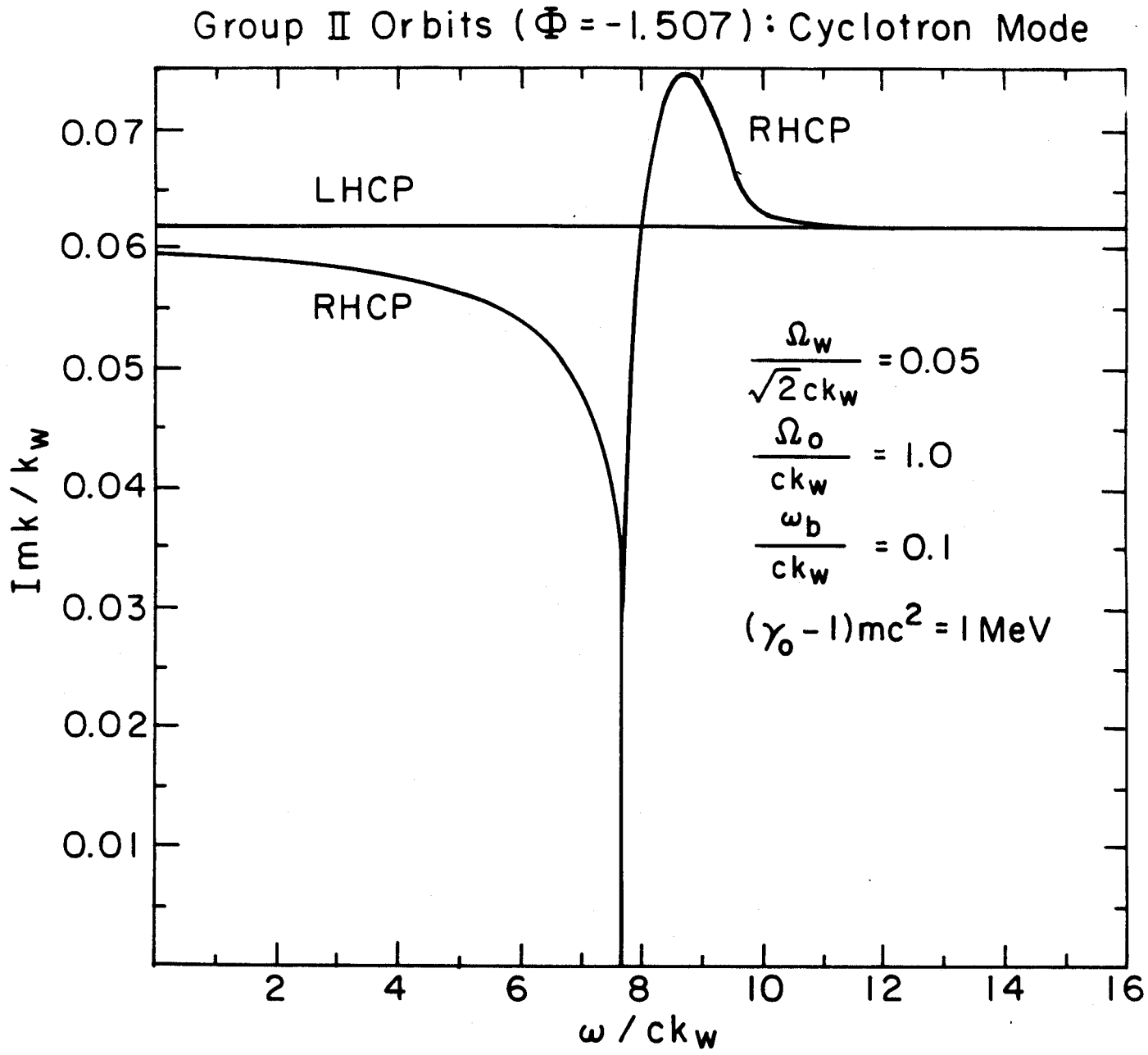
Group II Orbits ($\Phi = -1.507$) : Cyclotron Mode
RHCP
LHCP
RHCP
$\frac{\Omega_w}{\sqrt{2}ck_w} = 0.05$
$\frac{\Omega_o}{ck_w} = 1.0$
$\frac{\omega_b}{ck_w} = 0.1$
$(\gamma_o - 1)mc^2 = 1\,MeV$
Imk/k_w
ω/ck_w
0.07
0.06
0.05
0.04
0.03
0.02
0.01
2
4
6
8
10
12
14
16

Fig. 8